Geophysical Research Letters

RESEARCH LETTER
10.1029/2024GL108813

Why Do Oceanic Nonlinearities Contribute Only Weakly to Extreme El Niño Events?

Fangyu Liu[1,2], Jérôme Vialard[2], Alexey V. Fedorov[2,3], Christian Éthé[2], Renaud Person[4], Wenjun Zhang[1], and Matthieu Lengaigne[5]

[1]CIC-FEMD/ILCEC, Key Laboratory of Meteorological Disaster of Ministry of Education (KLME), Nanjing University of Information Science and Technology, Nanjing, China, [2]LOCEAN-IPSL, Sorbonne Université -CNRS-IRD-MNHN, Paris, France, [3]Department of Earth and Planetary Science, Yale University, New Haven, CT, USA, [4]Sorbonne Université, CNRS, IRD, MNHN, OSU Ecce Terra, LOCEAN-IPSL, Paris, France, [5]MARBEC, University of Montpellier, CNRS, IFREMER, IRD, Sète, France

Abstract Extreme El Niño events have outsized global impacts and control the El Niño Southern Oscillation (ENSO) warm/cold phases asymmetries. Yet, a consensus regarding the relative contributions of atmospheric and oceanic nonlinearities to their genesis remains elusive. Here, we isolate the contribution of oceanic nonlinearities by conducting paired experiments forced with opposite wind stress anomalies in an oceanic general circulation model, which realistically simulates extreme El Niño events and oceanic nonlinearities thought to contribute to ENSO skewness (Tropical Instability Waves (TIWs), Nonlinear Dynamical Heating (NDH)). Our findings indicate a weak contribution of oceanic nonlinearities to extreme El Niño events in the eastern Pacific, owing to compensatory effects between lateral (NDH and TIWs) and vertical processes. These results hold across different vertical mixing schemes and modifications of the upper-ocean heat budget mixed layer criterion. Our study reinforces previous research underscoring the pivotal role of atmospheric nonlinearities in shaping extreme El Niño events.

Plain Language Summary The El Niño-Southern Oscillation (ENSO) is the primary driver of year-to-year climate variations in the tropics and beyond. Originating from air-sea interactions in the tropical Pacific, ENSO oscillates between warm (El Niño) and cold (La Niña) phases, modulating sea surface temperature in the central and eastern equatorial Pacific. Occasionally, El Niño events intensify into "super" El Niño events, causing widespread impacts globally. Utilizing a state-of-the-art oceanic model, our research challenges previous results suggesting a strong oceanic contribution to the amplitude difference between "normal" and "super" El Niño events. Instead, our findings reveal that potential oceanic influences on "super" El Niño events tend to offset each other. This is consistent with recent research highlighting the crucial role of atmospheric processes in the transformation from a "normal" to a "super" El Niño.

Key Points:

- A state-of-the-art ocean model reproduces extreme El Niño events and the corresponding nonlinear oceanic processes realistically
- Contributions from oceanic nonlinearities are isolated using paired simulations forced by opposite wind stress anomalies
- Effects of oceanic nonlinearities on extreme El Niño events are small, due to compensation between lateral and vertical processes

Supporting Information:

Supporting Information may be found in the online version of this article.

Correspondence to:

J. Vialard,
jerome.vialard@ird.fr

Citation:

Liu, F., Vialard, J., Fedorov, A. V., Éthé, C., Person, R., Zhang, W., & Lengaigne, M. (2024). Why do oceanic nonlinearities contribute only weakly to extreme El Niño events? *Geophysical Research Letters*, *51*, e2024GL108813. https://doi.org/10.1029/2024GL108813

Received 14 FEB 2024
Accepted 21 MAY 2024

1. Introduction

Extreme El Niño events, such as in 1982–1983, 1997–1998 and 2015–2016 (Cai et al., 2017), are distinguished by a pronounced western Pacific warm pool eastward expansion. The associated widespread redistribution of atmospheric convection profoundly impacts climate, ecosystems and socioeconomics regionally and globally through atmospheric teleconnections (Beniche et al., 2023; Cai et al., 2012; Vincent et al., 2011). Additionally, extreme El Niño events are largely responsible for the asymmetry between the El Niño Southern Oscillation (ENSO) warm and cold phases (Bayr et al., 2024). Indeed, El Niño events exhibit eastward-shifted surface temperature signal with a greater amplitude than La Niña events (An et al., 2020; Deser & Wallace, 1987; Dommenget et al., 2013; Takahashi et al., 2011) as illustrated by the dipole pattern in Figure 1a (half sum of observed El Niño and La Niña composites). Figure 1b, which omits extreme events from the El Niño composite, reveals that three extreme El Niño events entirely account for the positively-skewed eastern equatorial Pacific sea surface temperature (SST) anomalies. This raises the question of processes that contribute to those extreme event large amplitudes.

ENSO asymmetries stem from nonlinearities within the coupled ocean-atmosphere system (e.g., An et al., 2020). The nonlinear dependence of tropical convection to SST results in precipitation and wind anomalies that are eastward-shifted and stronger during El Niño compared to La Niña (e.g., Graham & Barnett, 1987; Hoerling et al., 1997; Srinivas et al., 2022), thereby contributing to ENSO asymmetry (Choi et al., 2013; Frauen &

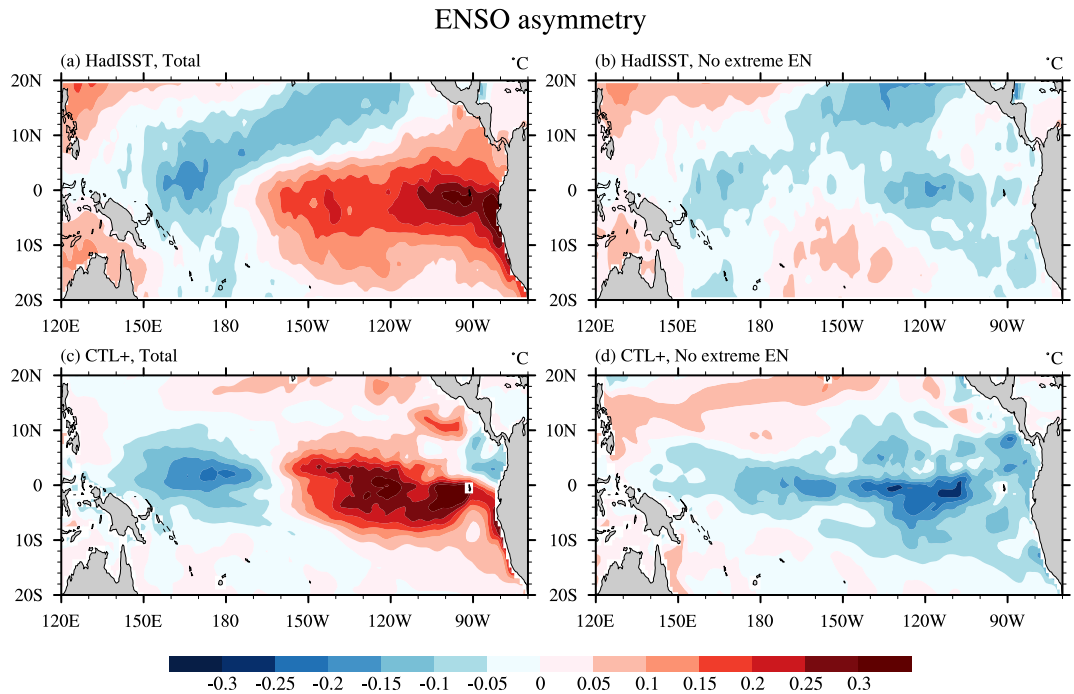

Figure 1. ENSO asymmetry (half sum of DJF El Niño and La Niña composites over 1980–2018, °C) for panel (a) HadISST and (c) the control ocean simulation CTL+, (b) and (d) as (a) and (c), but excluding the 1982, 1997 and 2015 extreme El Niño events from the asymmetry computation.

Dommenget, 2010; Geng et al., 2019; Kang & Kug, 2002; Ohba & Ueda, 2009) or specifically to extreme events (Srinivas et al., 2024; Takahashi et al., 2018). Westerly Wind Bursts (WWBs), are more frequent, intense, and eastward-shifted during warm events (Eisenman et al., 2005; Puy et al., 2015). WWBs thus increase the likelihood of extreme El Niño occurrences (e.g., Hu & Fedorov, 2017; Lengaigne et al., 2004; Puy et al., 2017; Yu & Fedorov, 2020, 2022) and contribute to ENSO asymmetry (Jin et al., 2007; Yu & Fedorov, 2022).

Oceanic nonlinearities provide alternative mechanisms for ENSO asymmetry and extreme El Niño occurrences. Tropical instability waves (TIWs) are eddies that form between the eastern Pacific equatorial cold tongue and warmer waters to the north (Willett et al., 2006). They warm the cold tongue through lateral advection (Menkes et al., 2006; Vialard et al., 2001), intensifying during La Niña and weakening during El Niño (Yu & Liu, 2003) and serving as negative feedback to ENSO (Vialard et al., 2001). TIWs weakly cool the cold tongue during El Niño but warm it more strongly during La Niña, potentially contributing to ENSO asymmetry (S. I. An, 2008; Imada & Kimoto, 2012). Vertical (An & Jin, 2004) and horizontal (Su et al., 2010) nonlinear dynamic heating (NDH), resulting from anomalous advection of temperature anomalies, is also thought to contribute to extreme El Niño events (Hayashi & Jin, 2017; Jin et al., 2003; Timmermann et al., 2003). Simple models also often incorporate a greater sensitivity of SST to positive than to negative thermocline depth anomalies as a source of ENSO asymmetry (e.g., Timmermann et al., 2003; Zebiak & Cane, 1987).

In summary, the extent to which oceanic and atmospheric nonlinearities respectively contribute to extreme El Niño events remains uncertain. Our previous study (Srinivas et al., 2024) suggested that atmospheric nonlinearities predominantly drive the amplitude difference between moderate and extreme El Niño events. In that study, atmospheric nonlinearities were isolated through paired ensemble simulations using an Atmospheric General Circulation Model (AGCM) forced with opposite SST anomalies, which were subsequently used to force simulations with an Ocean General Circulation Model (OGCM). However, the contribution of oceanic nonlinearities was not explicitly quantified. Our current investigation explicitly isolates oceanic nonlinearities and assesses their contribution to extreme El Niño events, using the same OGCM. We introduce the model physics and observational data sets in Section 2. We demonstrate the model's ability to reproduce extreme El Niño characteristics in Section 3. Section 4 explains our methodology for quantifying oceanic nonlinearities, reveals

their weak role and explains why they are weak based on a mixed layer heat budget. We summarize our findings, discuss their robustness, and address potential caveats associated with model biases and resolution in Section 5.

2. Data Sets and Control Simulation

We use monthly SST from the Hadley Centre Global Sea Ice and SST (HadISST) version 1.1 (Rayner, 2003), daily SST from the Microwave optimally interpolated (MW_OI) SST version 5.1 (Remote Sensing Systems, 2017), monthly sea surface height (SSH) and three-dimensional ocean currents from the European Centre for Medium-Range Weather Forecasts (ECMWF) Ocean re-analysis system 5 (ORAS5; Zuo et al., 2019), and daily surface currents from Ocean Surface Current Analyses (OSCAR; Bonjean & Lagerloef, 2002). The MW_OI/OSCAR data are available since 1998/1993 to present, respectively. The monthly anomalies are obtained by subtracting the 1980–2018 climatology.

We use the NEMO v3.6 (Nucleus for European Models of the Ocean, Madec et al., 2023) OGCM Orca1 (Deshayes et al., 2021) global configuration. It has a 1° horizontal resolution with a meridional resolution refinement to 1/3° in the equatorial band, and 75 vertical levels (1-m resolution at the surface, 10 to 20-m at typical equatorial Pacific thermocline depths). Vertical mixing is parameterized based on a vertical turbulent kinetic energy equation (Blanke & Delecluse, 1993), but we will show that our results are robust when using the generic length scale (GLS, Umlauf & Burchard, 2003; Umlauf et al., 2003) scheme.

Our control experiment spans from 1958 to 2018, initialized with temperature and salinity from the World Ocean Atlas 2018 (WOA18, Garcia et al., 2019) data and currents at rest. The study period is restricted to post-1980, leaving suffient time for the upper 1,000 m to adjust to forcing. This experiment is forced by the 3-hourly JRA55-do (Tsujino et al., 2018) interannual wind stresses. Net air-sea fluxes (Q) are parameterized as $\overline{Q} - \gamma\left(T - \overline{T}\right)$, where $\overline{Q}$ is the JRA55-do net heat flux climatology and the second term a relaxation of the model SST (T) to the observed HadISST SST climatology ($\overline{T}$), with a -15 $\mathrm{Wm^{-2}K^{-1}}$ relaxation coefficient γ. This method effectively approximates the neat surface fluxes interannual variations in the equatorial band (Vialard et al., 2001), as will be corroborated by the model's comparison with observed SST anomalies. Hereafter, we refer to this control experiment as CTL+. In Section 4, we will describe a paired experiment CTL− forced by the JRA55-do wind stress climatology minus interannual wind stresses (i.e., forced by opposite wind stress anomalies to those in the control experiment). The linear and nonlinear components of the oceanic response to wind stress anomalies can be obtained from CTL+ and CTL− (Section 4 and Text S1 in Supporting Information S1).

To diagnose the physical processes responsible for the SST evolution, we evaluate the ocean mixed layer heat budget, following Vialard et al. (2001) (details in supporting Text S2 in Supporting Information S1). At each timestep, temperature tendency terms are averaged vertically over the time-varying mixed layer, defined as the depth where potential density exceeds that at 10 m by 0.01 kg $\mathrm{m^{-3}}$. The total SST tendency is broken into contributions from (a) subsurface processes (Sub; including vertical advection, vertical mixing and entrainment), (b) air-sea flux forcing (For), (c) low-frequency lateral advection and (d) TIWs as in Vialard et al. (2001). Interannual low-frequency lateral advection anomalies are computed from monthly mean mixed layer current and temperature, and can be broken into linear ($-\overline{u}\partial_x T' - u'\partial_x \overline{T} - \overline{v}\partial_y T' - v'\partial_y \overline{T}$) and nonlinear $-u'\partial_x T' - v'\partial_y T'$, that is, lateral NDH) components. The TIWs budget contribution is obtained by subtracting low-frequency advection from total advection, and parameterized lateral mixing (a rather small contribution) is integrated to the effect of TIWs. The budget is closed.

We have computed vertically-integrated 0–50 m lateral NDH in ORAS5 for validation purposes. Available oceanic products or re-analyses outputs do not resolve TIWs well, and do not allow to compute TIWs-induced advection. Instead, we estimate the observed TIWs activity from the 60 days high-pass filtered daily MW_OI SST data, using a Lanczos filter. The map from Figure S4b in Supporting Information S1 is computed from the standard deviation of this high-pass filtered data over 1998–2018, while the TIWs index on, for example, Figure 2e corresponds to interannual anomalies of monthly standard deviation of that high-pass filtered data.

3. Model Evaluation

We first verify that our control experiment reproduces ENSO asymmetry and interannual variability. The simulated SST asymmetry (Figure 1c) deviates from observations (Figure 1a) poleward of 5°, because fluxes there force SST and not solely act as a negative feedback as in our simple formulation (not shown). It however

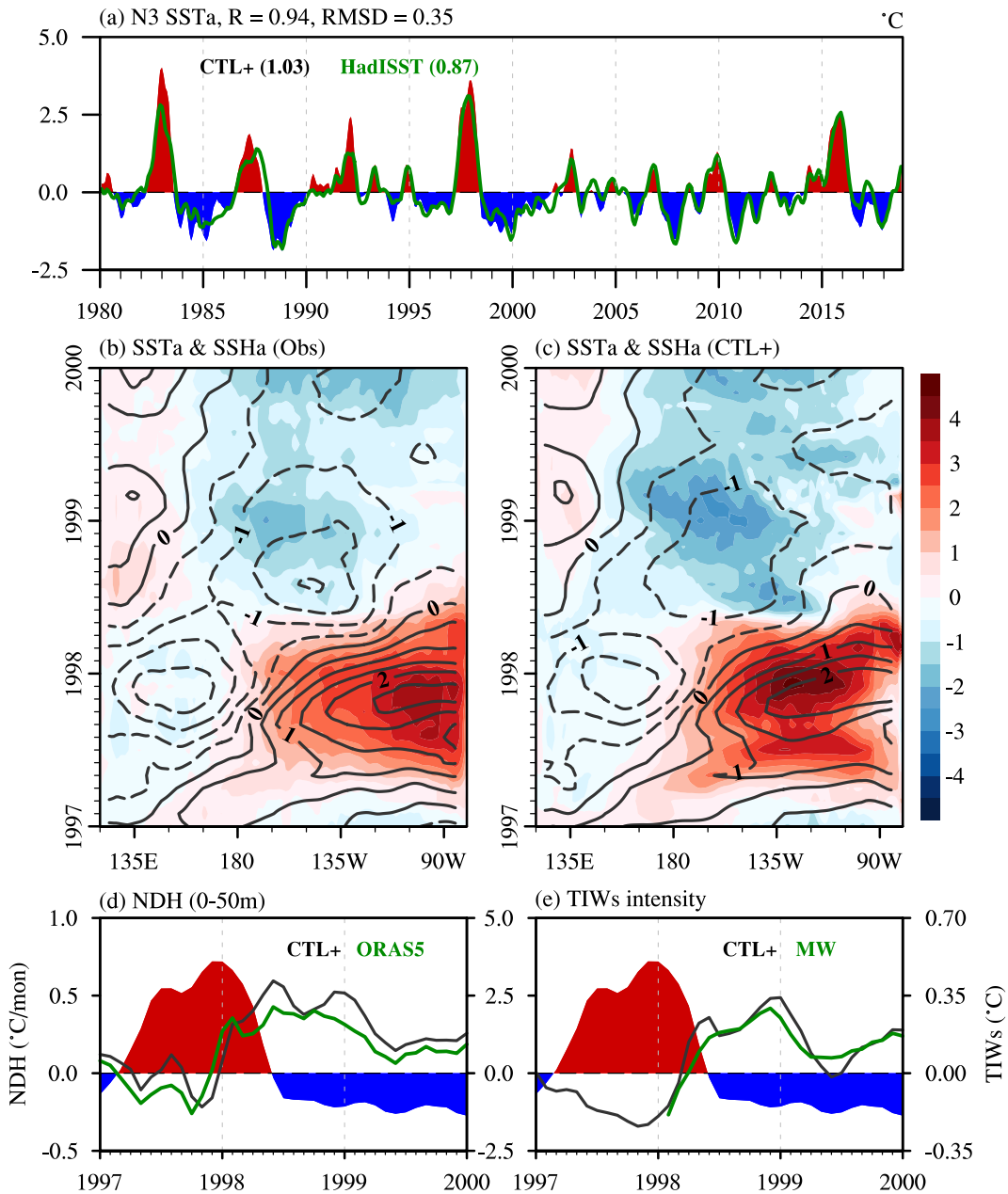

Figure 2. (a) Time series of Niño3 average Sea Surface Temperature (SST) anomalies for the CTL+ ocean simulation (red and blue shading; °C) and HadISST (green curve; °C). The number in brackets indicate the standard deviation of each curve, and their correlation and root mean square difference (RMSD) are indicated above. (b) Time-longitude section of observed SST (shading; °C) and SSH (contour; m) anomalies during 1997–1998. Panel (c) as panel (b), but for CTL+. (d) Time series of Niño3 average SST anomalies (red and blue shading; °C), 0–50 m average horizontal Nonlinear Dynamical Heating (NDH) in CTL+ (black curve; °C/month) and ORAS5 (green curve; °C/month). Panel (e) as panel (d), but for the CTL+ (black curve; °C) and Microwave OISST (green curve; °C) Tropical Instability Waves (TIWs) intensity index (see Section 2). A 3-month smoothing is applied to panels (a), (d) and (e).

displays a similar east-west dipole pattern to observations within the equatorial band and hence reproduces the stronger and eastward shifted El Niño relative to La Niña events. Consistent with observations, the three modeled extreme El Niño events explain all of the ENSO asymmetry in the central and eastern Pacific (Figures 1b–1d). The model also has realistic SST, surface currents and thermocline depth (from the 20°C isotherm) climatologies (Figure S1 in Supporting Information S1).

Our net heat flux parameterization involves no information on observed SST interannual variability. The model Niño3 (5°S–5°N, 90°W–150°W) SST anomalies can thus be validated against observations (Figure 2a), demonstrating realistic variations (0.94 correlation). The model reproduces the La Niña amplitude accurately, but overestimates the amplitude of extreme El Niño events (overestimated std of 1.06 vs. 0.87°C). This overestimation may be attributed to our linear surface heat flux feedback: the eastern Pacific shortwave feedback nonlinearity indeed limits El Niño amplitude (e.g., Lloyd et al., 2012). However, El Niño peaks are better represented post-1993.

We further assess the control experiment during the 1997–1998 extreme El Niño event. The ocean model reproduces the initial eastward propagation of positive SST and SSH anomalies from the western to the central Pacific (Figures 2b and 2c), in response to WWBs in late 1996 and early 1997 (e.g., McPhaden, 1999). Additionally, the model reproduces the thermocline tilt mode, exhibiting a raised thermocline in the western and deepened thermocline in the eastern Pacific through summer and fall, along with the associated eastern Pacific warming that culminates in boreal winter. Our simulation however develops an unrealistic SST peak during midsummer, whose origin is unclear. Nonetheless, the model subsequently reproduces the progressive SST warming and SSH decrease in the central and eastern equatorial Pacific, followed by an abrupt transition to La Niña in 1998. The high pattern correlations between Figures 2b and 2c (0.97 for SSH and 0.90 for SST anomalies) underscore this very good agreement. The model also reproduces the observed equatorial SST and SSH anomalies during and after the 1982–1983 and 2015–2016 extreme El Niño events very well (Figures S2 and S3 in Supporting Information S1).

NDH and TIWs represent the two primary oceanic mechanisms proposed to account for eastern Pacific SST positive skewness (An et al., 2020). It is therefore important for our study of oceanic nonlinearities contribution to ENSO that our model reproduces NDH and TIWs well. The model and observations display remarkably similar NDH (0–50 m Niño3 $-\boldsymbol{u}'\partial_x\boldsymbol{T}' - \boldsymbol{v}'\partial_y\boldsymbol{T}'$) evolutions during and after the 1997–1998 El Niño (Figure 2d). During and shortly after this ENSO peak, NDH warms the eastern Pacific as emphasized by previous studies (e.g., Hayashi & Jin, 2017; Jin et al., 2003). However, prior to that, NDH in fact acts as a cooling term in the model and ORAS5 re-analysis, obscuring its integrated effect over the entire event. Figures S2 and S3 in Supporting Information S1 further demonstrate the agreement between modeled and observed NDH for the 1982–1983 and 2015–2016 events (with a slight overestimation that does not question our results: we will come back to this point in the discussion).

Prior to early 1998, observed TIWs intensity interannual anomalies are unavailable. However, they agree with the model by indicating suppressed TIWs activity during the end of the El Niño, followed by an activity increase during the 1998 La Niña (Figure 2e). Modeled and observed TIWs activity also display a very similar pattern (Figures S4a and S4b in Supporting Information S1) and interannual evolution (Figure S4c in Supporting Information S1, 0.94 correlation), including during 2015–2016 (Figure S3d in Supporting Information S1). Overall, our control simulation accurately reproduces extreme El Niño events and the observed NDH and TIWs, laying the groundwork for the quantification of oceanic nonlinearities in the next section.

4. Weak Role of Oceanic Nonlinearities During Extreme El Niño Events

Below, we separate the linear and nonlinear contributions of the oceanic response to ENSO wind stress forcing. Let us illustrate this for SST and note the CTL + SST $\boldsymbol{T}(\boldsymbol{\tau}')$ and that of CTL− (forced by opposite wind stress anomalies $-\boldsymbol{\tau}'$, Figure 3a) $\boldsymbol{T}(-\boldsymbol{\tau}')$. Due to the OGCM nonlinear dynamics, $\boldsymbol{T}(-\boldsymbol{\tau}')$ is not the opposite of $\boldsymbol{T}(\boldsymbol{\tau}')$ (Figure 3b); instead, a nonlinear correction arises. Therefore, we decompose the CTL + SST $\boldsymbol{T}(\boldsymbol{\tau}')$ (Figure 3c, black curve) into two components: $\frac{1}{2}\left[\boldsymbol{T}(\boldsymbol{\tau}') - \boldsymbol{T}(-\boldsymbol{\tau}')\right]$ (Figure 3c, gray curve) and $\frac{1}{2}\left[\boldsymbol{T}(\boldsymbol{\tau}') + \boldsymbol{T}(-\boldsymbol{\tau}')\right]$ (Figure 3c, red curve). In principle, the former gives the sum of odd and the latter of even terms in the Taylor expansion of $\boldsymbol{T}(\boldsymbol{\tau}')$. In practice, they yield the linear and quadratic contributions, respectively (Figure S5; Srinivas et al., 2024). We hence term them linear and nonlinear parts of the oceanic response to wind stress. This methodology is used throughout to separate the CTL+solution into a linear and nonlinear part, and detailed in supporting Text S1 in Supporting Information S1).

Figure 3d displays the time series of Niño3 average CTL + SST anomalies, alongside their linear and nonlinear contributions. The linear SST response to wind stress closely aligns with total SST variations throughout 1980–2018, accounting for 93% of the total standard deviation. Oceanic nonlinearities barely contribute to La Niña

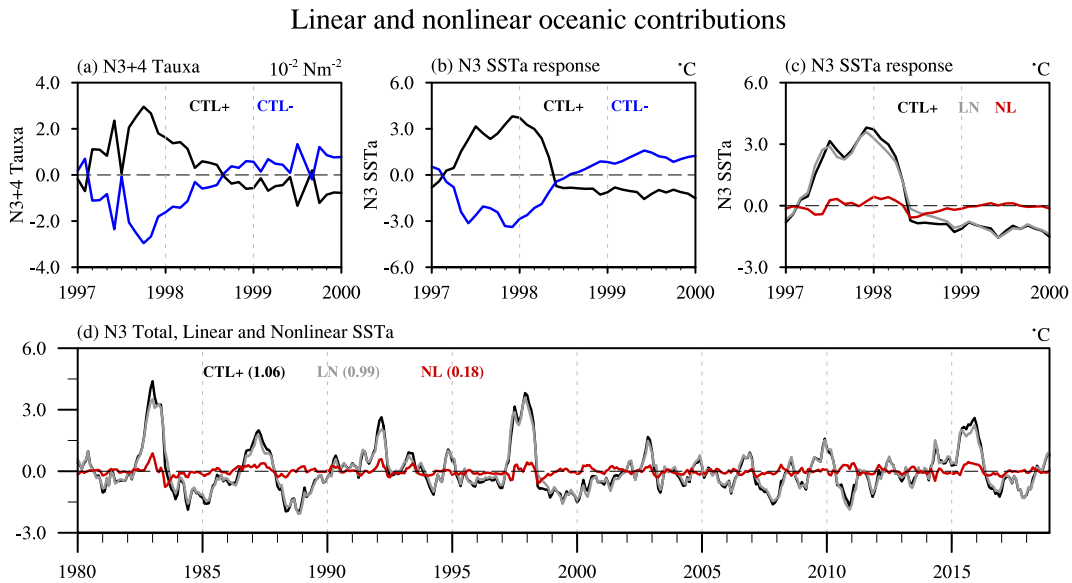

Figure 3. 1997–2000 time series of (a) Niño3 + 4 (5°S–5°N, 160°E–90°W) average zonal wind stress anomalies (10^{-2} Nm^{-2}) from the CTL+ (black curve) and CTL− (blue curve) ocean simulations. Niño3 average sea surface temperature (SST) anomalies (°C) in (b) CTL+ (black curve) and CTL− (blue curve), (c) CTL+ simulation SST anomaly (°C; black curve), and its decomposition into the linear (gray curve) and nonlinear (red curve) components of the response to anomalous wind stress. The linear component is obtained from the half difference of CTL+ and CTL− and the nonlinear component from their half sum (see Section 4). Panel(d) as panel (c), but for 1980–2018. The numbers within brackets indicate the standard deviation of each curve.

events and most El Niño events, except in 1997–1998, 1982–1983 and 2015–2016, where they respectively contribute to 5.7%, 16.7% and 14.7% of the November–January Niño3 SST anomalies. Although these contributions are not completely negligible, they are much weaker than the 40%–50% contribution from atmospheric nonlinearities highlighted by Srinivas et al. (2024). Our result hence indicates that the oceanic response to ENSO forcing is predominantly linear, even during extreme El Niño events. This result contrasts with previous studies discussing the TIWs/NDH large contributions to extreme El Niño amplitude.

To investigate the reason for this limited influence of net oceanic nonlinearity, we use a Niño3 region mixed layer heat budget (supporting Text S2 in Supporting Information S1). Employing a similar approach as above, we break each budget term into its linear and nonlinear components. Figures 4a–4c display the nonlinear component of Niño3-averaged heat budget terms as a function of equatorial zonal wind stress anomalies. Given the predominantly linear SST response to wind stress (Figure 3d), the SST nonlinear tendency is rather small (Figure 4a) compared with the linear tendency (Figure S6 in Supporting Information S1). The nonlinear contribution to the SST tendency is further broken into contributions from lateral advection (NDH + TIWs, Figure 4b) and vertical processes (exchanges between the mixed layer and the atmosphere/subsurface, both processes involving vertical mixing, Figure 4c). The absence of nonlinearity in the total trend (Figure 4a) arises from a counterbalance between a positive quadratic nonlinearity associated with lateral processes (Figure 4b) and a negative quadratic nonlinearity associated with vertical processes (Figure 4c). The former has been extensively discussed in studies proposing that NDH and TIWs contribute to the positive ENSO skewness in the eastern Pacific. We will discuss mechanisms for the latter in Section 5.

Let us examine this compensation mechanism for the three extreme El Niño events. The December minus January Niño3 SST anomalies over 1997, 1982 and 2015 are broken into linear and nonlinear contributions, and the nonlinear contributions further broken into lateral and vertical processes (Figures 4d–4f). Oceanic nonlinearities contribute most during 2015 (25%), with a weaker contribution (less than 15%) for the two other events. The 2015 event stands out due to its notably weaker eastern Pacific warming, largely attributable to the absence of anomalous warming by TIWs. For the 1982 and 1997 extreme events, the weak contribution of nonlinearities results from a compensation between a large nonlinear warming through lateral processes and cooling through vertical processes (Figures 4a–4c). While NDH induces cooling for the 1997 event (as noted earlier from

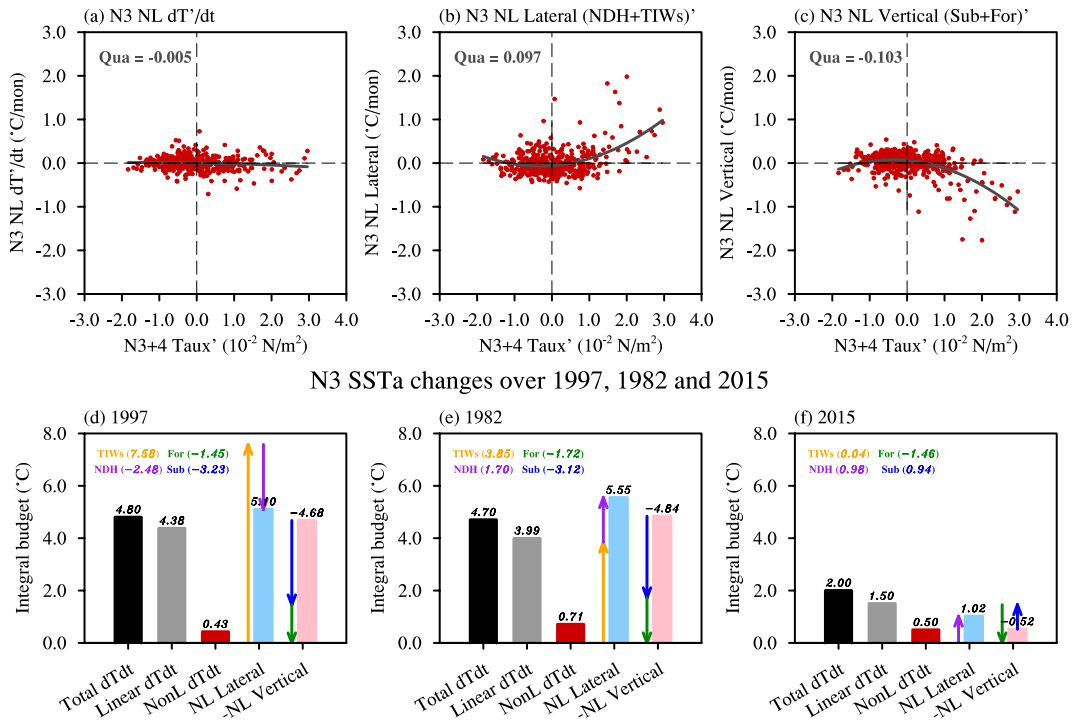

Figure 4. Scatterplot of Niño3 average mixed layer heat budget nonlinear terms (red dots; °C/mon) as a function of Niño3 + 4 average zonal wind stress anomalies (Taux, 10^{-2} Nm^{-2}): (a) mixed layer temperature tendency (dT/dt), (b) lateral contributions (sum of NDH and Tropical instability waves (TIWs)), (c) vertical contributions (sum of the subsurface and air-sea fluxes). Quadratic fits are indicated as gray lines on panels (a)–(c), with the quadratic coefficient indicated on the top left of each panel. Contributions to December minus January Sea Surface Temperature (SST) anomalies for panel (d) 1997, (e) 1982 and (f) 2015: total SST change (black) and contributions from linear (gray) and nonlinear (red) oceanic processes. The nonlinear contribution is further broken into lateral (blue, comprising TIWs in orange and NDH in purple) and vertical (pink, multiplied by −1, comprising subsurface in blue and air-sea fluxes in green). The positive (negative) values are indicated by upward (downward) arrows.

Figure 2d), the total nonlinear advection (TIWs and NDH) yields a warming for both events. Overall, the compensation between lateral and vertical nonlinearities explains why oceanic net nonlinearity is subdued for the 1982 and 1997 events. Additionally, individual contributions to oceanic nonlinearities are weak for the 2015 event, questioning whether this event should be classified as extreme (Paek et al., 2017).

5. Summary and Discussion

Here, we have explicitly diagnosed oceanic nonlinearities from OGCM realistic experiments, concluding that their contribution to extreme El Niño amplitude in the eastern Pacific is weak. This finding corroborates the results of Srinivas et al. (2024), who indicated that most of the eastern Pacific SST anomalies positive skewness can be attributed to the wind stress nonlinear response to SST. This is also consistent with prior studies emphasizing atmospheric nonlinearities in extreme El Niño events (e.g., Takahashi et al., 2018) and ENSO asymmetry (e.g., Choi et al., 2013; Frauen & Dommenget, 2010; Geng et al., 2019; Kang & Kug, 2002; Ohba & Ueda, 2009; Yu & Fedorov, 2022). There is however an apparent discrepancy with previous studies analyzing the role of oceanic nonlinearities. Most of these studies highlight the TIWs/NDH contribution to the ENSO positive skewness from observations (e.g., S. I. An, 2008; Hayashi & Jin, 2017; Jin et al., 2003), and we find a similar positive quadratic nonlinearity characterizing these processes (Figure 4b). These studies typically demonstrate the TIWs/NDH impact on ENSO by introducing a representation of these particular oceanic nonlinearities into simple models (e.g., S. I. An, 2008; Jin et al., 2003; Timmermann et al., 2003), thus neglecting other oceanic nonlinearities. In contrast, our OGCM includes all possible sources of oceanic nonlinearities, enabling us to conclude that the net effect of oceanic nonlinearities is weak due to the strong compensation between lateral (NDH + TIWs) and vertical nonlinearities.

Why does vertical oceanic mixing induces nonlinear cooling during extreme El Niño events (Figure 4c)? Recent eastern Pacific microstructure measurements indicate that upper ocean mixing decreases during El Niño events and increases during La Niña (Warner & Moum, 2019), consistent with our control simulation (Figure S7 in Supporting Information S1). Further analyses (not shown) indicate that air-sea fluxes and vertical mixing both contribute to the negative quadratic nonlinearity in vertical processes. This can be understood as follows. Reduced mixing during El Niño concentrates the negative feedback associated with air-sea fluxes over a shallow layer, enhancing its cooling efficiency and favoring El Niño weakening. To explain the contribution of vertical mixing, let us represent vertical heat fluxes at the bottom of the mixed layer as $-\kappa\Delta T$ where κ represents a positive mixing velocity and ΔT the mixed layer minus subsurface temperature. During El Niño, κ' and $\Delta T'$ are negative, leading to linear terms ($-\overline{\kappa}\Delta T' - \kappa'\Delta\overline{T}$) that warm as expected, but a nonlinear $-\kappa'\Delta T'$ term that cools. This cooling term is activated during extreme El Niño, while the La Niña amplitude does not seem sufficient to activate it (Figure 4c). Consequently, the processes involving vertical ocean mixing weaken strong El Niño events.

The robustness of our results hinges on the model ability to realistically simulate equatorial processes. NDH is slightly overestimated in our model, but this should increase the oceanic nonlinearity contribution to ENSO positive skewness, and hence does not question our results. Our model also displays a cold and shallow thermocline bias in the eastern and central Pacific (Figure S1 in Supporting Information S1), which may accentuate vertical processes at the expanse of lateral ones. However, the very good representation of interannual variability in our control simulation suggests a reasonable representation of ENSO dynamics in our experiment. Furthermore, the weak overall contribution of oceanic nonlinearities is robust when conducting the paired experiments with an alternative vertical mixing scheme (Figure S8 in Supporting Information S1) or by analyzing the upper-ocean heat budget over the time-varying mixing layer, as defined from the mixing scheme, rather than mixed layer (Figure S9 in Supporting Information S1). In all instances, a compensation between lateral and vertical oceanic nonlinearities is evident. It would be interesting to investigate this compensation mechanism in the light of the TIWs intensification over recent decades (Wang et al., 2024). The robustness of the limited role of oceanic nonlinearities for extreme ENSO events should also be investigated at higher resolution and in a coupled framework.

Data Availability Statement

HadISST is available through https://www.metoffice.gov.uk/hadobs/hadisst/data/download.html. MW_OI SST is obtained by https://data.remss.com/SST/daily/mw/v05.1/netcdf/. ORAS5 data set can be request through https://cds.climate.copernicus.eu/cdsapp#!/dataset/reanalysis-oras5?tab=form. OSCAR data set is provided by https://podaac.jpl.nasa.gov/dataset/OSCAR_L4_OC_1deg.

Acknowledgments
FL was supported by a Chinese Scholarship Council Grant (202209040023) during her stay at LOCEAN. We thank Yona Silvy for developing the flexible framework for applying perturbations to the forcing in the NEMO experiments. All figures were prepared in NCL, the related code and OGCM simulations are available on request from FL. This work was supported by the French Agence Nationale pour la Recherche (ANR) ARiSE Grant (ANR-18-CE01-0012). AVF is supported by the ARCHANGE project (ANR-18-MPGA-0001, France) and Grants from NOAA (NA20OAR4310377) and US Department of Energy (DE-SC0023134).

References

An, S.-I. (2008). Interannual variations of the tropical ocean instability wave and ENSO. *Journal of Climate*, *21*(15), 3680–3686. https://doi.org/10.1175/2008jcli1701.1

An, S.-I., & Jin, F.-F. (2004). Nonlinearity and asymmetry of ENSO. *Journal of Climate*, *17*(12), 2399–2412. https://doi.org/10.1175/1520-0442(2004)017<2399:naaoe>2.0.co;2

An, S. I., Tziperman, E., Okumura, Y. M., & Li, T. (2020). ENSO irregularity and asymmetry. In *El Niño southern oscillation in a changing climate* (pp. 153–172).

Bayr, T., Lübbecke, J. F., Vialard, J., & Latif, M. (2024). Equatorial pacific cold tongue bias degrades the simulation of ENSO asymmetry in climate models. *Journal of Climate*. in revision.

Beniche, M., Vialard, J., Lengaigne, M., Voldoire, A., Srini, G., & Hall, N. M. J. (2023). A distinct and reproducible teleconnection pattern over North America during extreme El Niño events. *Scientific Reports*, *14*(1), 2457. https://doi.org/10.1038/s41598-024-52580-9

Blanke, B., & Delecluse, P. (1993). Variability of the tropical Atlantic Ocean simulated by a general circulation model with two different mixed-layer physics. *Journal of Physical Oceanography*, *23*(7), 1363–1388. https://doi.org/10.1175/1520-0485(1993)023<1363:vottao>2.0.co;2

Bonjean, F., & Lagerloef, G. S. E. (2002). Diagnostic model and analysis of the surface currents in the tropical Pacific Ocean. *Journal of Physical Oceanography*, *32*(10), 2938–2954. https://doi.org/10.1175/1520-0485(2002)032<2938:dmaaot>2.0.co;2

Cai, W., Lengaigne, M., Borlace, S., Collins, M., Cowan, T., McPhaden, M. J., et al. (2012). More extreme swings of the South Pacific convergence zone due to greenhouse warming. *Nature*, *488*(7411), 365–369. https://doi.org/10.1038/nature11358

Cai, W., Wang, G., Santoso, A., Lin, X., & Wu, L. (2017). Definition of extreme El Niño and its impact on projected increase in extreme El Niño frequency. *Geophysical Research Letters*, *44*(21). https://doi.org/10.1002/2017gl075635

Choi, K.-Y., Vecchi, G. A., & Wittenberg, A. T. (2013). ENSO transition, duration, and amplitude asymmetries: Role of the nonlinear wind stress coupling in a conceptual model. *Journal of Climate*, *26*(23), 9462–9476. https://doi.org/10.1175/jcli-d-13-00045.1

Deser, C., & Wallace, J. M. (1987). El Niño events and their relation to the southern oscillation: 1925–1986. *Journal of Geophysical Research*, *92*(C13), 14189–14196. https://doi.org/10.1029/jc092ic13p14189

Deshayes, J., Ethé, C., Mignot, J., & Levy, C. (2021). Full information on the eORCA1 grid (mesh_mask) used in IPSL-CM6A-LR configuration [Dataset]. *Zenodo*. https://doi.org/10.5281/zenodo.4432892

Dommenget, D., Bayr, T., & Frauen, C. (2013). Analysis of the non-linearity in the pattern and time evolution of El Niño southern oscillation. *Climate Dynamics*, *40*(11–12), 2825–2847. https://doi.org/10.1007/s00382-012-1475-0

Eisenman, I., Yu, L., & Tziperman, E. (2005). Westerly wind bursts: ENSO's tail rather than the dog? *Journal of Climate*, *18*(24), 5224–5238. https://doi.org/10.1175/jcli3588.1

Frauen, C., & Dommenget, D. (2010). El Niño and La Niña amplitude asymmetry caused by atmospheric feedbacks. *Geophysical Research Letters*, *37*(18). https://doi.org/10.1029/2010gl044444

Garcia, H. E., Boyer, T. P., Baranova, O. K., Locarnini, R. A., Mishonov, A. V., Grodsky, A., et al. (2019). In A. Mishonov (Ed.), *World Ocean Atlas 2018: Product documentation*. Technical Editor.

Geng, T., Cai, W., Wu, L., & Yang, Y. (2019). Atmospheric convection dominates genesis of ENSO asymmetry. *Geophysical Research Letters*, *46*(14), 8387–8396. https://doi.org/10.1029/2019gl083213

Graham, N. E., & Barnett, T. P. (1987). Sea surface temperature, surface wind divergence, and convection over tropical oceans. *Science*, *238*(4827), 657–659. https://doi.org/10.1126/science.238.4827.657

Hayashi, M., & Jin, F. F. (2017). Subsurface nonlinear dynamical heating and ENSO asymmetry. *Geophysical Research Letters*, *44*(24). https://doi.org/10.1002/2017gl075771

Hoerling, M. P., Kumar, A., & Zhong, M. (1997). El Niño, La Niña, and the nonlinearity of their teleconnections. *Journal of Climate*, *10*(8), 1769–1786. https://doi.org/10.1175/1520-0442(1997)010<1769:enolna>2.0.co;2

Hu, S., & Fedorov, A. V. (2017). The extreme El Niño of 2015–2016: The role of westerly and easterly wind bursts, and preconditioning by the failed 2014 event. *Climate Dynamics*, *52*(12), 7339–7357. https://doi.org/10.1007/s00382-017-3531-2

Imada, Y., & Kimoto, M. (2012). Parameterization of tropical instability waves and examination of their impact on ENSO characteristics. *Journal of Climate*, *25*(13), 4568–4581. https://doi.org/10.1175/jcli-d-11-00233.1

Jin, F.-F., Kug, J.-S., An, S.-I., & Kang, I.-S. (2003). A near-annual coupled ocean-atmosphere mode in the equatorial Pacific Ocean. *Geophysical Research Letters*, *30*(2), 1080. https://doi.org/10.1029/2002gl015983

Jin, F.-F., Lin, L., Timmermann, A., & Zhao, J. (2007). Ensemble-mean dynamics of the ENSO recharge oscillator under state-dependent stochastic forcing. *Geophysical Research Letters*, *34*(3), L03807. https://doi.org/10.1029/2006gl027372

Kang, I.-S., & Kug, J.-S. (2002). El Niño and La Niña sea surface temperature anomalies: Asymmetry characteristics associated with their wind stress anomalies. *Journal of Geophysical Research*, *107*(D19), 4372. https://doi.org/10.1029/2001jd000393

Lengaigne, M., Guilyardi, E., Boulanger, J.-P., Menkes, C., Delecluse, P., Inness, P., et al. (2004). Triggering of El Niño by westerly wind events in a coupled general circulation model. *Climate Dynamics*, *23*(6), 601–620. https://doi.org/10.1007/s00382-004-0457-2

Lloyd, J., Guilyardi, E., & Weller, H. (2012). The role of atmosphere feedbacks during ENSO in the CMIP3 models. Part III: The shortwave flux feedback. *Journal of Climate*, *25*(12), 4275–4293. https://doi.org/10.1175/jcli-d-11-00178.1

Madec, G., Bell, M., Blaker, A., Bricaud, C., Bruciaferri, D., & Castrillo, M., et al. (2023). NEMO ocean engine reference manual. *Zenodo*. https://doi.org/10.5281/zenodo.8167700

McPhaden, M. J. (1999). Genesis and evolution of the 1997-98 El nino. *Science*, *283*(5404), 950–954. https://doi.org/10.1126/science.283.5404.950

Menkes, C. E. R., Vialard, J. G., Kennan, S. C., Boulanger, J.-P., & Madec, G. V. (2006). A modeling study of the impact of tropical instability waves on the heat budget of the eastern equatorial Pacific. *Journal of Physical Oceanography*, *36*(5), 847–865. https://doi.org/10.1175/jpo2904.1

Ohba, M., & Ueda, H. (2009). Role of nonlinear atmospheric response to SST on the asymmetric transition process of ENSO. *Journal of Climate*, *22*(1), 177–192. https://doi.org/10.1175/2008jcli2334.1

Paek, H., Yu, J. Y., & Qian, C. (2017). Why were the 2015/2016 and 1997/1998 extreme El Niños different? *Geophysical Research Letters*, *44*(4), 1848–1856. https://doi.org/10.1002/2016gl071515

Puy, M., Vialard, J., Lengaigne, M., & Guilyardi, E. (2015). Modulation of equatorial Pacific westerly/easterly wind events by the Madden–Julian oscillation and convectively-coupled Rossby waves. *Climate Dynamics*, *46*(7–8), 2155–2178. https://doi.org/10.1007/s00382-015-2695-x

Puy, M., Vialard, J., Lengaigne, M., Guilyardi, E., DiNezio, P. N., Voldoire, A., et al. (2017). Influence of westerly wind events stochasticity on El Niño amplitude: The case of 2014 vs. 2015. *Climate Dynamics*, *52*(12), 7435–7454. https://doi.org/10.1007/s00382-017-3938-9

Rayner, N. A., Parker, D. E., Horton, E. B., Folland, C. K., Alexander, L. V., Rowell, D. P., et al. (2003). Global analyses of sea surface temperature, sea ice, and night marine air temperature since the late nineteenth century. *Journal of Geophysical Research*, *108*(D14), 4407. https://doi.org/10.1029/2002jd002670

Remote Sensing Systems. (2017). MWIR optimum interpolated SST data set. Ver. 5.0. PO.DAAC, CA, USA. https://doi.org/10.5067/GHMWI-4FR05

Srinivas, G., Vialard, J., Lengaigne, M., Izumo, T., & Guilyardi, E. (2022). Relative contributions of sea surface temperature and atmospheric nonlinearities to ENSO asymmetrical rainfall response. *Journal of Climate*, *35*(12), 3725–3745. https://doi.org/10.1175/jcli-d-21-0257.1

Srinivas, G., Vialard, J., Liu, F., Voldoire, A., Izumo, T., Guilyardi, E., & Lengaigne, M. (2024). Dominant contribution of atmospheric nonlinearities to ENSO asymmetry and extreme El Niño events. *Scientific Reports*, *14*(1), 8122. https://doi.org/10.1038/s41598-024-58803-3

Su, J., Zhang, R., Li, T., Rong, X., Kug, J. S., & Hong, C.-C. (2010). Causes of the El Niño and La Niña amplitude asymmetry in the equatorial eastern Pacific. *Journal of Climate*, *23*(3), 605–617. https://doi.org/10.1175/2009jcli2894.1

Takahashi, K., Karamperidou, C., & Dewitte, B. (2018). A theoretical model of strong and moderate El Niño regimes. *Climate Dynamics*, *52*(12), 7477–7493. https://doi.org/10.1007/s00382-018-4100-z

Takahashi, K., Montecinos, A., Goubanova, K., & Dewitte, B. (2011). ENSO regimes: Reinterpreting the canonical and Modoki El Niño. *Geophysical Research Letters*, *38*(10), L10704. https://doi.org/10.1029/2011gl047364

Timmermann, A., Jin, F.-F., & Abshagen, J. (2003). A nonlinear theory for El Niño Bursting. *Journal of the Atmospheric Sciences*, *60*(1), 152–165. https://doi.org/10.1175/1520-0469(2003)060<0152:antfen>2.0.co;2

Tsujino, H., Urakawa, S., Nakano, H., Small, R. J., Kim, W. M., Yeager, S. G., et al. (2018). JRA-55 based surface dataset for driving ocean–sea-ice models (JRA55-do). *Ocean Modelling*, *130*, 79–139. https://doi.org/10.1016/j.ocemod.2018.07.002

Umlauf, L., & Burchard, H. (2003). A generic length-scale equation for geophysical turbulence models. *Journal of Marine Research*, *61*(2), 235–265. https://doi.org/10.1357/002224003322005087

Umlauf, L., Burchard, H., & Hutter, K. (2003). Extending the k–ω turbulence model towards oceanic applications. *Ocean Modelling*, *5*(3), 195–218. https://doi.org/10.1016/s1463-5003(02)00039-2

Vialard, J., Menkes, C., Boulanger, J.-P., Delecluse, P., Guilyardi, E., McPhaden, M. J., & Madec, G. (2001). A model study of oceanic mechanisms Affecting equatorial Pacific Sea Surface temperature during the 1997–98 El Niño. *Journal of Physical Oceanography*, *31*(7), 1649–1675. https://doi.org/10.1175/1520-0485(2001)031<1649:amsoom>2.0.co;2

Vincent, E. M., Lengaigne, M., Menkes, C. E., Jourdain, N. C., Marchesiello, P., & Madec, G. (2011). Interannual variability of the South Pacific Convergence Zone and implications for tropical cyclone genesis. *Climate Dynamics*, *36*(9–10), 1881–1896. https://doi.org/10.1007/s00382-009-0716-3

Wang, M., Xie, S.-P., Sasaki, H., Nonaka, M., & Du, Y. (2024). Intensification of Pacific tropical instability waves over the recent three decades. *Nature Climate Change*, *14*(2), 163–170. https://doi.org/10.1038/s41558-023-01915-x

Warner, S. J., & Moum, J. N. (2019). Feedback of mixing to ENSO phase change. *Geophysical Research Letters*, *46*(23), 13920–13927. https://doi.org/10.1029/2019gl085415

Willett, C. S., Leben, R. R., & Lavín, M. F. (2006). Eddies and tropical instability waves in the eastern tropical Pacific: A review. *Progress in Oceanography*, *69*(2–4), 218–238. https://doi.org/10.1016/j.pocean.2006.03.010

Yu, J.-Y., & Liu, W. T. (2003). A linear relationship between ENSO intensity and tropical instability wave activity in the eastern Pacific Ocean. *Geophysical Research Letters*, *30*(14), 1735. https://doi.org/10.1029/2003gl017176

Yu, S., & Fedorov, A. V. (2020). The role of westerly wind bursts during different seasons versus ocean heat recharge in the development of extreme El Niño in climate models. *Geophysical Research Letters*, *47*(16), e2020GL088381. https://doi.org/10.1029/2020gl088381

Yu, S., & Fedorov, A. V. (2022). The essential role of westerly wind bursts in ENSO dynamics and extreme events quantified in model "wind stress shaving" experiments. *Journal of Climate*, *35*(22), 7519–7538. https://doi.org/10.1175/jcli-d-21-0401.1

Zebiak, S. E., & Cane, M. A. (1987). A model El Nino–southern oscillation. *Monthly Weather Review*, *115*(10), 2262–2278. https://doi.org/10.1175/1520-0493(1987)115<2262:ameno>2.0.co;2

Zuo, H., Balmaseda, M. A., Tietsche, S., Mogensen, K., & Mayer, M. (2019). The ECMWF operational ensemble reanalysis–analysis system for ocean and sea ice: A description of the system and assessment. *Ocean Science*, *15*(3), 779–808. https://doi.org/10.5194/os-15-779-2019